

Hopping-disorder-induced effects upon the two-Magnon Raman Scattering spectrum in an Antiferromagnet

Saurabh Basu *

Department of Physics, Indian Institute of Technology, Kanpur 208016, India

Two-magnon Raman scattering intensity is obtained for two-dimensional spin-1/2 antiferromagnets in presence of hopping disorder. A consistent mode assignment scheme is prescribed which essentially establishes a correspondence between the hopping-disordered and the pure system. It is seen that a minute amount of disorder in hopping leads to a good agreement of the Raman lineshape experimentally obtained for the copper-oxide insulators such as La_2CuO_4 . Also it is observed that a considerable asymmetry with respect to the two-magnon peak appears and the spectral intensity persisting much beyond $4J$ (where the joint magnon density of states peaks). This has been argued earlier by us [S. Basu and A. Singh, Phys. Rev. B, **53**, 6406 (1996)] to be arising due to highly asymmetric magnon-energy renormalization because of a cooperative effect arising from local correlation in hopping disorder.

I. INTRODUCTION

Recently it was put forward by Nori et al. [1] that the exchange disorder caused by zero-point lattice vibration can account for various experimentally observed features of the two-magnon Raman intensity lineshape. In their approach the exchange disorder is looked upon as an interaction between the lattice excitation (i.e. phonons) and the spin excitations (i.e. magnons) which induces changes δJ_{ij} , in the exchange integral J . An estimate of the mean square deviation $\langle (\frac{\delta J_{ij}}{J})^2 \rangle$ is made and to make a comparison with the experimental data the corresponding value is considered to be as high as 0.5 (in units of J). It has been suspected [2] that such a large variation in J appears physically unreasonable and questioned that whether more moderate values of $\langle \frac{\delta J_{ij}}{J} \rangle$ are sufficient to achieve agreement with experiments. Essentially what one obtains is that the coupling of phonons to the spin excitations leads to the broadening of a two-magnon peak, the asymmetry of the lineshape about its maximum towards the higher energy regime and appearance of scattering intensity in forbidden geometries like A_{1g} , B_{2g} etc.

Earlier, we have investigated, [3] the effect of lattice fluctuation induced hopping disorder in the context of Mott-Hubbard AF where the hopping term t_{ij} include random terms. The Hubbard Hamiltonian in this case can be written as,

$$H = - \sum_{\langle ij \rangle, \sigma} (t + \delta t_{ij}) (a_{i\sigma}^\dagger \hat{a}_{j,\sigma} + \text{h.c.}) + U \sum_i \hat{n}_{i\uparrow} \hat{n}_{i\downarrow} \quad (1)$$

$$P \left(\frac{\delta t_{ij}}{t} \right) = \frac{1}{\sqrt{2\pi}\sigma} \exp \left[-\frac{(\delta t_{ij}/t)^2}{2\sigma} \right] \quad (2)$$

where the random terms δt_{ij} 's for each bond are chosen independently from a gaussian distribution and the distribution width $\sqrt{\sigma}$ measures the strength of disorder. There we have examined both perturbatively

* e-mail : snbasu@iitk.ac.in

and using the exact eigenstate method - effects of hopping disorder on magnon energies, their wavefunctions and on the density of states (DOS). In both schemes, the spin-wave energies are obtained at the Random Phase Approximation (RPA) level. We have obtained a strong renormalization in energy of the high energy magnon modes, arising from locally correlated hopping, which results in appreciable one-magnon DOS well beyond the maximum spin-wave energy $2J$ for the pure system. This result has got important implications in explaining the experimentally observed Raman spectrum.

To obtain the Raman scattering intensity we need to consider the imaginary part of the full two-magnon propagator which in turn requires the knowledge of spin-wave energies. For a finite size system these energies are obtained numerically at the RPA level in presence of disorder using the exact eigenstate method discussed in detail elsewhere [4]. Following a prescription of the mode assignments discussed in section III, it is possible to obtain the symmetry factor required for the B_{1g} scattering geometry (in Appendix A, we discuss the calculation of the symmetry factor in the B_{1g} geometry corresponding to the pure case). It is observed that even for a sufficiently small strength of disorder, $\sigma = 0.01$, (much smaller than the values considered by Nori et al. [1]) though the Raman spectrum on the lower energy side is weakly affected, there is a substantial change in the higher frequency regime and a good agreement is obtained with the experimental data. This confirms our earlier statement [3] that if indeed the randomness in hopping due to zero-point lattice fluctuation is playing a key-role in explaining the long standing puzzling feature of the Raman lineshape regarding the asymmetry, then it essentially arises from the highly asymmetric magnon-energy renormalization.

II. CONFIGURATION AVERAGING OF THE TWO-MAGNON PROPAGATOR

The Fleury-Loudon (FL) Hamiltonian which represents the interaction between the photon and the spin pairs can be written as,

$$H_R = A \sum_{\mathbf{r}, \hat{\delta}} (\mathbf{E}_{inc} \cdot \hat{\delta}) \cdot (\mathbf{E}_{sc} \cdot \hat{\delta}) \mathbf{S}(\mathbf{r}) \cdot \mathbf{S}(\mathbf{r} + \hat{\delta}) \quad (3)$$

Where the \mathbf{E}_{inc} and \mathbf{E}_{sc} are the incident and the scattered electric field vectors, $\hat{\delta}$ is the unit vector connecting nearest neighbour (NN) sites of opposite sublattices and A is a constant. The sum over \mathbf{r} ensures that the spin excitations have net zero momentum as the incoming photon has essentially zero momentum. For calculation of the Raman intensity one needs to consider the correlation function of the spin pair operator,

$$P_{\hat{\delta}} = \sum_{\mathbf{r}} \mathbf{S}(\mathbf{r}) \cdot \mathbf{S}(\mathbf{r} + \hat{\delta}) \quad (4)$$

Now for the B_{1g} symmetry we have,

$$\mathbf{E}_{inc} \sim \hat{x} - \hat{y}$$

$$\mathbf{E}_{sc} \sim \hat{x} + \hat{y}.$$

So that the Hamiltonian assumes the form,

$$H_R \sim \sum_{\mathbf{r}, p=\pm 1} \mathbf{S}(\mathbf{r}) \cdot \{\mathbf{S}(\mathbf{r} + p\hat{x}) - \mathbf{S}(\mathbf{r} + p\hat{y})\} \quad (5)$$

Now let us consider the diagram representing (Fig. 1) the interaction between the magnons in real space. The interaction between the magnons excited at sites \mathbf{r}_1 and $\mathbf{r}_1 + \mu$ can be written as,

$$\hat{V}_{int} = -J \sum_{\mathbf{r}_1, \mu} S^-(\mathbf{r}_1) S^+(\mathbf{r}_1) S^-(\mathbf{r}_1 + \mu) S^+(\mathbf{r}_1 + \mu) \quad (6)$$

where μ connects to NN sites of the opposite sublattice. The form of the interaction indicates that the propagators on either sides of the interaction line are coupled as μ can connect both in the \hat{x} and \hat{y} direction. But they can be decoupled if one rewrites the interaction term as (see Fig. 1),

$$\hat{V}_{\text{int}} = -J \sum_{\mathbf{r}_1} S^-(\mathbf{r}_1) S^+(\mathbf{r}_1) \left[S_{O_1}^-(\mathbf{r}_1) S_{O_1}^+(\mathbf{r}_1) + S_{O_2}^-(\mathbf{r}_1) S_{O_2}^+(\mathbf{r}_1) \right. \\ \left. + S_{O_3}^-(\mathbf{r}_1) S_{O_3}^+(\mathbf{r}_1) + S_{O_4}^-(\mathbf{r}_1) S_{O_4}^+(\mathbf{r}_1) \right] \quad (7)$$

where the 4 operators are defined in the following way,

$$S_{O_1}^\pm(\mathbf{r}) = \frac{1}{2} \sum_p \{S^\pm(\mathbf{r} + p\hat{x}) - S^\pm(\mathbf{r} + p\hat{y})\}$$

$$S_{O_2}^\pm(\mathbf{r}) = \frac{1}{2} \sum_p \{S^\pm(\mathbf{r} + p\hat{x}) + S^\pm(\mathbf{r} + p\hat{y})\}$$

$$S_{O_3}^\pm(\mathbf{r}) = \frac{1}{2} \sum_p \{pS^\pm(\mathbf{r} + p\hat{x}) - pS^\pm(\mathbf{r} + p\hat{y})\}$$

$$S_{O_4}^\pm(\mathbf{r}) = \frac{1}{2} \sum_p \{pS^\pm(\mathbf{r} + p\hat{x}) + pS^\pm(\mathbf{r} + p\hat{y})\}$$

where the +sign and the -sign in the superscript refers to raising and lowering operators respectively. The first two operators correspond to B_{1g} and A_{1g} symmetry factors respectively. Hence explicitly we write them as $S_{B_{1g}}^\pm$ and $S_{A_{1g}}^\pm$ for our convenience. In this new notation the interaction term looks like,

$$\hat{V}_{\text{int}} = -J \sum_{\mathbf{r}_1} S^-(\mathbf{r}_1) S^+(\mathbf{r}_1) \left[S_{B_{1g}}^-(\mathbf{r}_1) S_{B_{1g}}^+(\mathbf{r}_1) + S_{A_{1g}}^-(\mathbf{r}_1) S_{A_{1g}}^+(\mathbf{r}_1) \right. \\ \left. + S_{O_3}^-(\mathbf{r}_1) S_{O_3}^+(\mathbf{r}_1) + S_{O_4}^-(\mathbf{r}_1) S_{O_4}^+(\mathbf{r}_1) \right] \quad (8)$$

Having written the interaction term we proceed to define the spin-wave propagators in different scattering geometries. In Fig. 1 the spin raising and lowering operators at \mathbf{r} and $\mathbf{r} + \hat{\delta}$ are denoted by $S^+(\mathbf{r})$ and $S_{B_{1g}}^-(\mathbf{r})$ and those at \mathbf{r}' and $\mathbf{r}' + \hat{\delta}'$ are denoted by $S^-(\mathbf{r}')$ and $S_{B_{1g}}^+(\mathbf{r}')$. This immediately suggests that $\hat{\delta}$ and $\hat{\delta}'$ which connect NN pairs are fixed in space and we can write the spin-wave propagators as,

$$\chi^{-+}(\mathbf{r}, \mathbf{r}') = \langle \psi_G | S^-(\mathbf{r}) S^+(\mathbf{r}') | \psi_G \rangle \quad (9)$$

corresponding to the upper line and,

$$\chi_{B_{1g}}^{+-}(\mathbf{r}, \mathbf{r}') = \langle \psi_G | S_{B_{1g}}^+(\mathbf{r}) S_{B_{1g}}^-(\mathbf{r}') | \psi_G \rangle \quad (10)$$

corresponding to the lower one in Fig. 1. Now the time-ordered two-magnon propagator in the B_{1g} geometry can be defined as,

$$G_{B_{1g}}(\omega) = -i \int dt e^{i\omega(t-t')} \langle \psi_G | T \left[\sum_{\mathbf{r}, \mathbf{r}'} S^-(\mathbf{r}, t) S_{B_{1g}}^+(\mathbf{r}, t) S^+(\mathbf{r}', t') S_{B_{1g}}^-(\mathbf{r}', t') \right] | \psi_G \rangle \quad (11)$$

For calculating the Raman intensity first consider the non-interacting limit of the two-magnon propagator,

$$G_{B_{1g}}^0(\omega) = i \int \frac{d\omega_1}{2\pi} \sum_{\mathbf{r}, \mathbf{r}'} \chi^{-+}(\mathbf{r}, \mathbf{r}', \omega_1) \chi_{B_{1g}}^{+-}(\mathbf{r}, \mathbf{r}', \omega - \omega_1) \quad (12)$$

The configuration averaged two-magnon Raman propagator is given by,

$$\overline{G_{B_{1g}}^0(\omega)} = i \int \frac{d\omega_1}{2\pi} \sum_{\mathbf{r}, \mathbf{r}'} \overline{\chi^{-+}(\mathbf{r}, \mathbf{r}', \omega_1) \chi_{B_{1g}}^{+-}(\mathbf{r}, \mathbf{r}', \omega - \omega_1)} \quad (13)$$

We can decouple the two propagators if we neglect the corrections arising due to exchange between the magnons. This allows us to write,

$$\overline{G_{B_{1g}}^0(\omega)} = i \int \frac{d\omega_1}{2\pi} \sum_{\mathbf{r}, \mathbf{r}'} \overline{\chi^{-+}(\mathbf{r}, \mathbf{r}', \omega_1)} \overline{\chi_{B_{1g}}^{+-}(\mathbf{r}, \mathbf{r}', \omega - \omega_1)} \quad (14)$$

Having done the configuration averaging of $G^0(\omega)$ one can proceed to calculate the two-magnon Raman intensity which is obtained from imaginary part of $\overline{G(\omega)}$ where,

$$\overline{G(\omega)} = \left[\frac{G_0(\omega)}{1 + JG_0(\omega)} \right] \quad (15)$$

We can neglect the vertex corrections since they appear only at the second order level and hence proportional to the fourth power of the disorder strength *i.e.* $\left(\frac{\delta t}{t}\right)^4$ (in reference [5] this result is shown explicitly for the on-site (diagonal) disorder case and calculation of the vertex correction is discussed). So for weak disorder, the correction will be insignificant. This enables to write,

$$\overline{G(\omega)} = \left[\frac{\overline{G_0(\omega)}}{1 + J\overline{G_0(\omega)}} \right] \quad (16)$$

Now it is shown in Appendix A that the B_{1g} symmetry factor viz. $(\cos q_x - \cos q_y)^2$ corresponding to the pure case is obtained by Fourier transforming the non-interacting two-magnon propagator $G_{B_{1g}}^0$ (Eq. 12). This symmetry factor is important for calculating the two-magnon Raman scattering intensity. It can also be noted that due to the form of the interaction *i.e.* presence of both B_{1g} and A_{1g} terms in \hat{V}_{int} , off-diagonal combinations of different scattering geometries in $G^0(\omega)$ are possible. In that case the symmetry factor will contain contributions from different geometries. We can see it clearly if one considers,

$\langle S_{\mathbf{r}}^+(B_{1g}) S_{\mathbf{r}'}^-(A_{1g}) \rangle$ which when Fourier transformed yields,

$$\sum_q (\cos q_x - \cos q_y)(\cos q_x + \cos q_y) \chi^{+-}(q, \omega) \quad (17)$$

But this symmetry term can be shown to be identically equal to zero for all frequencies because of the symmetry present in the magnetic Brillouin Zone. Hence the only terms which survive are the ones that are diagonal in scattering geometries [6].

III. MODE ASSIGNMENTS

Here we want to establish a one-to-one correspondence between the pure system and the one in presence of hopping disorder. For doing this we calculate the magnon modes using the exact eigenstate method for a 10×10 system in absence of disorder in the strong-coupling limit ($U/t = 200$). This procedure of obtaining the magnon modes numerically has been discussed in reference [4]. These modes thus obtained

are assigned a pair of mode numbers n_x and n_y which are related the wavevectors q_x and q_y via the relation $q_{x/y} = \frac{2\pi}{L} n_{x/y}$ in the translationally invariant (pure) case. The numbers n_x and n_y are chosen such that the corresponding q_x and q_y are restricted to the upper-half (first two quadrants) of the Brillouin Zone (BZ) where q_x is allowed to have both positive and negative values (ranging from $-\pi$ to $+\pi$) whereas q_y is assigned only positive values (from 0 to π). The other half of the BZ does not need to be considered as the q_x and q_y values (or equivalently the n_x and n_y) lying within the region specified (see Fig. 2) are sufficient to label all the modes. The Goldstone mode or the lowest energy mode is assigned with the mode numbers $n_x = 0$, $n_y = 0$, the second collective mode with $n_x = 1$, $n_y = 0$ (or equivalently $n_x = 0$, $n_y = 1$), the third one with $n_x = 1$, $n_y = 1$ and so on. Having done with the assigning scheme it is now possible to form the symmetry factor for the B_{1g} scattering geometry which is $\phi_n^2 = [\cos(\frac{2\pi}{L}n_x) - \cos(\frac{2\pi}{L}n_y)]^2$. This symmetry factor is necessary for calculating the two-magnon Raman intensity. The consistency of the mode assigning scheme is checked by re-evaluating the magnon energies using the mode numbers via the relation $\omega_n = 2J\sqrt{1 - \gamma_n^2}$ where $\gamma_n = \frac{1}{2}[\cos(\frac{2\pi}{L}n_x) + \cos(\frac{2\pi}{L}n_y)]$ and $J = \frac{4t^2}{U} = 0.02$ (i.e. $U/t = 200$). The energies thus obtained show excellent agreement with the ones calculated from the exact eigenstate method for the pure case. The same mode assignments are expected to be carried over for the intermediate coupling regime. We show the comparison between the energies calculated numerically from the exact eigenstate method and the ones evaluated by using the analytical expression relevant to the intermediate- U regime ($U/t = 10$) viz.

$$\omega_n = 2J \left[(1 - \gamma_n^2) - \frac{t^2}{\Delta^2} \{ 6 + 3 \cos\left(\frac{2\pi}{L}\right) n_x \cos\left(\frac{2\pi}{L}\right) n_y - 9\gamma_n^2 \} \right]^{1/2} \quad (18)$$

in Table I. We establish the correspondence between the pure and the disordered system by assuming the same assigning scheme continues to work for the disordered system. We show the mode energies for the disordered system ($\sigma = 0.1$) for a particular configuration in Table II. We also notice that the degeneracy of the modes is lifted due to the presence of disorder and the low energy modes are not significantly affected whereas there is a considerable effect towards the higher energy side. To substantiate this result regarding the nature of the high energy modes, we have examined the magnon wavefunction for the high-energy modes and find that these modes are strongly localised in certain regions of the lattice [3]. In reference [3] it is also mentioned that the localization of the high-energy magnon modes occurs in those regions of the lattice where the locally-averaged hopping strength is significantly higher than the bulk average, so that the local magnetization, which goes as $\sim U/t$ is low. This is shown in Fig. 3.

IV. CALCULATION OF THE TWO-MAGNON RAMAN INTENSITY

As before, [7] we can express the propagator in terms of it's non-interacting components $G_0(\omega)$. The mode assignments allows us to write $G_0(\omega)$ in a 2×2 matrix form with the mode energies and the symmetry factors are labeled by the mode numbers $n(= \sqrt{n_x^2 + n_y^2})$. Hence we can sum up the perturbation series in powers of the interaction between the magnons and which yields,

$$[G_n(\omega)] = \frac{[G_{0n}]}{1 + J[G_{0n}]} \quad (19)$$

As in reference [7] the above equation is written in terms of the matrix elements,

$$\begin{aligned} [G_{0n}(\omega)]_{AA} &= A_n, \\ [G_{0n}(\omega)]_{BB} &= B_n \quad \text{and} \\ [G_{0n}(\omega)]_{AB} &= [G_{0n}(\omega)]_{BA} = C_n \end{aligned}$$

$$\overline{G_n(\omega)} = \frac{A_n + B_n + 2C_n + 2J(A_n B_n - C_n^2)}{(1 + J A_n)(1 + J B_n) - J^2 C_n^2} \quad (20)$$

where A_n , B_n and C_n are defined as,

$$\begin{aligned} A_n &= \frac{1}{n} \sum_n m^2 \phi_n^2 \left(\frac{2J}{\omega_n} \right)^2 \left[a_n^2 - \left(\frac{\omega_n}{2J} \right)^2 - \left(\frac{a_n \omega}{2J} \right) + \frac{1}{2} \left(\frac{\omega}{2J} \right)^2 \right] \left[\frac{1}{\omega - 2\omega_n} - \frac{1}{\omega + 2\omega_n} \right] \\ B_n &= \frac{1}{n} \sum_n m^2 \phi_n^2 \left(\frac{2J}{\omega_n} \right)^2 \left[a_n^2 - \left(\frac{\omega_n}{2J} \right)^2 + \left(\frac{a_n \omega}{2J} \right) + \frac{1}{2} \left(\frac{\omega}{2J} \right)^2 \right] \left[\frac{1}{\omega - 2\omega_n} - \frac{1}{\omega + 2\omega_n} \right] \\ C_n &= \frac{1}{n} \sum_n m^2 \phi_n^2 \left(\frac{2J}{\omega_n} \right)^2 [b^2 \gamma_n^2] \left[\frac{1}{\omega - 2\omega_n} - \frac{1}{\omega + 2\omega_n} \right] \end{aligned}$$

where,

$$\begin{aligned} m &= 1 - 2 \frac{t^2}{\Delta^2}, \quad a_n = 1 - \frac{t^2}{\Delta^2} \left\{ 3 + \frac{3}{2} \cos\left(\frac{2\pi}{L} n_x\right) \cos\left(\frac{2\pi}{L} n_y\right) + \gamma_n^2 \right\} \quad \text{and} \\ b &= 1 - \frac{11}{2} \frac{t^2}{\Delta^2} \end{aligned}$$

In Fig. 4 we have shown the Raman scattering spectra in the B_{1g} symmetry as a function of transferred photon frequency ω (in units of J) for a system size 10×10 in presence of disorder ($\sigma = 0.1$) and $U/t = 10$. It is noticed that the linewidth to peak position ratio is even higher than unity, whereas the experimentally value is closed to 0.38 [8]. This shows clearly that the strength of disorder σ (or equivalently the mean square deviation $\langle (\delta J_{ij})^2 \rangle$) does not need to be as large as 0.1 in order to get an agreement with the experimentally observed data for the Raman spectrum. Fig. 5 shows the same plot for more moderate values of σ viz $\sigma = 0.01$ and 0.03 . The spectral lineshape for the pure case ($\sigma = 0$) is included for comparison. This plot is reminiscent of the magnon DOS shown in Fig. 2 in reference [3]. There we have considered much larger strengths of disorder ($\sigma = 0.1$ and 0.3). It can be observed that the linewidth to peak position ratio increases from 0.283 corresponding to the pure case to 0.37 for $\sigma = 0.01$ and 0.410 for $\sigma = 0.03$ whereas the position of the peak roughly stays the same in all the cases. So it looks like $\sigma = 0.01$ roughly corresponds to the value that is needed for parameterizing disorder strength in order to obtain agreement with the experimentally obtained Raman lineshape. Also it is seen that in presence of disorder there is a pronounced asymmetry in the higher frequency region of the spectrum and a considerable intensity is observed all the way upto $6J$ and even more. This can be explained by arguing that the high energy magnon modes are strongly affected due to a cooperative effect arising from local correlations of hopping disorder, which resulted in an appreciable one-magnon DOS beyond the maximum energy $2J$ for the pure system [3]. So it seems that a much lesser value of the disorder strength can actually account for the puzzling features of the Raman lineshape. Finally, in Fig. 6 we plot the scattering spectrum in the strong coupling limit ($U/t = 100$) for various disorder strengths viz. $\sigma = 0.01$, 0.03 and 0.1 in order to draw comparisons with the results obtained by Nori et al. [1] since their work deals with the strong coupling limit *i.e.* $U/t \rightarrow \infty$. The linewidth to peak position ratio in this case comes out to be 0.333, 0.406 and 1 corresponding to $\sigma = 0.01$, 0.03 and 0.1 . Also there is a pronounced asymmetry with respect to the two-magnon peak in the higher frequency regime. To obtain an idea about the asymmetry we measure the quantity $I(\omega = 4J)/I_{max}(\omega)$. This has a value close to 0.4 which agrees very well with the corresponding quantity obtained from the experiments done on La_2CuO_4 [8]. Nori et al. obtained agreement with experiments for $\sigma_J \sim 0.5J$ (they have defined σ_J in units of J) which is much more than what we have considered. This can be explained by noting that their Quantum Monte Carlo (QMC) calculations of the Raman spectrum for a $S = 1/2$ Heisenberg antiferromagnet in the B_{1g} scattering geometry reveals a much lesser linewidth to peak-position ratio (~ 0.176) since in their calculation the intrinsic magnon damping [7] has not been taken into account (remember we obtained 0.283 for the corresponding quantity [7] which is much closer to the experimental value 0.38 than that of Nori *et al.*). This explains the reason why they need a much bigger width (σ) in the distribution of the exchange constant J so as to have an agreement with experiments. In fact, the evaluation of the different spectral moments of the Raman lineshape due to Singh *et al.* [8] shows the ratio of the second moment to that of the first one (which is like the linewidth to peak-position ratio) as 0.23 which tallies very well with the experimental value 0.28.

In conclusion, we have studied the effects of hopping disorder on the two-magnon Raman intensity using the magnon energies calculated numerically using the exact eigenstate analysis. The energies for the disordered

case are assumed to have a one-to-one correspondence with the ones in the pure case. This correspondence is established by assigning mode numbers n_x and n_y which are related to the momentum labels via the relation $q_{x/y} = (\frac{2\pi}{L})n_{x/y}$. The validity of the assigning scheme is checked for the pure case by re-evaluating the mode energies using the mode numbers and hence comparing them with the ones obtained numerically. Once the consistency of the assigning scheme is checked, the numbers can be used to determine the symmetry factors which are required for calculating the Raman intensity in different scattering geometries. For the Raman lineshape in the B_{1g} in presence of a small amount of disorder (σ as small as 0.01) symmetry it is observed that the lineshape broadens and alongwith there appears a substantial asymmetry towards the higher frequency side while the low-energy modes are weakly affected. It is also observed that the spectral intensity persists even beyond $6J$ where the joint magnon DOS diverges at $4J$. We also obtained a good agreement for the linewidth and asymmetry of the two-magnon profile observed experimentally from the Raman studies on cuprate insulators for $\sigma = 0.01$. This clearly reflects the role of zero-point fluctuations of the lattice to explain the anomalous features appearing in Raman spectrum for the cuprate antiferromagnets via a highly asymmetric magnon energy renormalization arising due to correlation of hopping disorder.

APPENDIX A

Here we find an expression for the symmetry factor appropriate to the B_{1g} scattering geometry. The Fleury-Loudon Hamiltonian for the B_{1g} scattering geometry is written as (see Eq. 5),

$$H = A \sum_{\mathbf{r}, p=\pm 1} \mathbf{S}(\mathbf{r}) \cdot \{\mathbf{S}(\mathbf{r} + p\hat{x}) - \mathbf{S}(\mathbf{r} + p\hat{y})\} \quad (21)$$

The two-magnon propagator in the non-interacting limit for this case is,

$$G_0(\omega) = i \int \frac{d\omega_1}{2\pi} \sum_{\mathbf{r}, \mathbf{r}'} \chi^{+-}(\mathbf{r}, \mathbf{r}', \Omega_1) \chi_{B_{1g}}^{+-}(\tilde{\mathbf{r}}, \tilde{\mathbf{r}}', \omega - \omega_1) \quad (22)$$

where \mathbf{r}, \mathbf{r}' denote lattice sites and $\tilde{\mathbf{r}} = \mathbf{r} + \hat{\delta}$, $\tilde{\mathbf{r}}' = \mathbf{r}' + \hat{\delta}'$, where $\hat{\delta}/\hat{\delta}'$ connect to the sites neighbouring to \mathbf{r} and \mathbf{r}' in all the four directions i.e. $\hat{\delta}/\hat{\delta}'$ can be $p\hat{x}$ and $p\hat{y}$ with $p = \pm 1$. Also the spin raising and lowering operators forming the propagator is shown in the Fig. 7.

Clearly $\chi_{B_{1g}}^{+-}$ consists of 16 terms with $\hat{\delta}$ and $\hat{\delta}'$ having all possible combinations which are enumerated below (the energy dependence is dropped temporarily).

$$\begin{aligned} \chi_{B_{1g}}^{+-}(\tilde{\mathbf{r}}, \tilde{\mathbf{r}}') = & \chi^{+-}(\mathbf{r} + \hat{x}, \mathbf{r}' + \hat{x}) + \chi^{+-}(\mathbf{r} + \hat{x}, \mathbf{r}' - \hat{x}) \\ & - \chi^{+-}(\mathbf{r} + \hat{x}, \mathbf{r}' + \hat{y}) - \chi^{+-}(\mathbf{r} + \hat{x}, \mathbf{r}' - \hat{y}) \\ & + \chi^{+-}(\mathbf{r} - \hat{x}, \mathbf{r}' + \hat{x}) + \chi^{+-}(\mathbf{r} - \hat{x}, \mathbf{r}' - \hat{x}) \\ & - \chi^{+-}(\mathbf{r} - \hat{x}, \mathbf{r}' + \hat{y}) - \chi^{+-}(\mathbf{r} - \hat{x}, \mathbf{r}' - \hat{y}) \\ & - \chi^{+-}(\mathbf{r} + \hat{y}, \mathbf{r}' + \hat{x}) - \chi^{+-}(\mathbf{r} + \hat{y}, \mathbf{r}' - \hat{x}) \\ & + \chi^{+-}(\mathbf{r} + \hat{y}, \mathbf{r}' + \hat{y}) + \chi^{+-}(\mathbf{r} + \hat{y}, \mathbf{r}' - \hat{y}) \\ & - \chi^{+-}(\mathbf{r} - \hat{y}, \mathbf{r}' + \hat{x}) - \chi^{+-}(\mathbf{r} - \hat{y}, \mathbf{r}' - \hat{x}) \\ & + \chi^{+-}(\mathbf{r} - \hat{y}, \mathbf{r}' + \hat{y}) + \chi^{+-}(\mathbf{r} - \hat{y}, \mathbf{r}' - \hat{y}) \end{aligned} \quad (23)$$

To obtain the symmetry factor one has to Fourier transform all the 16 terms in $G_0(\omega)$. As an example, the calculations for the first two terms are shown below,

(1) The first term is,

$$i \int \frac{d\omega_1}{2\pi} \sum_{\mathbf{r}, \mathbf{r}'} \chi^{-+}(\mathbf{r}, \mathbf{r}') \chi^{+-}(\mathbf{r} + \hat{x}, \mathbf{r}' + \hat{x})$$

Taking the Fourier Transform,

$$i \int \frac{d\omega_1}{2\pi} \sum_{\mathbf{r}, \mathbf{r}'} \sum_{q, q'} \chi^{-+}(q) e^{iq \cdot (\mathbf{r} - \mathbf{r}')} \chi^{+-}(q') e^{iq' \cdot (\mathbf{r} - \mathbf{r}')}$$

Which can be written as,

$$i \int \frac{d\omega_1}{2\pi} \sum_q \chi^{-+}(q) \chi^{+-}(-q)$$

(2) And the second term,

$$i \int \frac{d\omega_1}{2\pi} \sum_{\mathbf{r}, \mathbf{r}'} \chi^{-+}(\mathbf{r}, \mathbf{r}') \chi^{+-}(\mathbf{r} + \hat{x}, \mathbf{r}' - \hat{x})$$

Fourier Transforming the above quantity yields,

$$i \int \frac{d\omega_1}{2\pi} \sum_{\mathbf{r}, \mathbf{r}'} \sum_{q, q'} \chi^{-+}(q) e^{iq \cdot (\mathbf{r} - \mathbf{r}')} \chi^{+-}(q') e^{iq' \cdot (\mathbf{r} - \mathbf{r}' - 2\hat{x})}$$

Which is equivalent to,

$$i \int \frac{d\omega_1}{2\pi} \sum_q \chi^{-+}(q) \chi^{+-}(-q) e^{-2iq\hat{x}}$$

Likewise we can calculate the contributions from the other 14 terms and all of them combine to give,

$$G_0(\omega) = i \int \frac{d\omega_1}{2\pi} \sum_q \chi^{-+}(q, \omega_1) \chi^{+-}(-q, \omega - \omega_1) [(\cos q_x - \cos q_y)^2] \quad (24)$$

Hence the symmetry factor used in the B_{1g} geometry is $(\cos q_x - \cos q_y)^2$. By taking the appropriate signs (positive) for the spin operators corresponding to the lower line in Fig. 7 for the A_{1g} geometry, it is trivial to show that the symmetry factor is $(\cos q_x + \cos q_y)^2$.

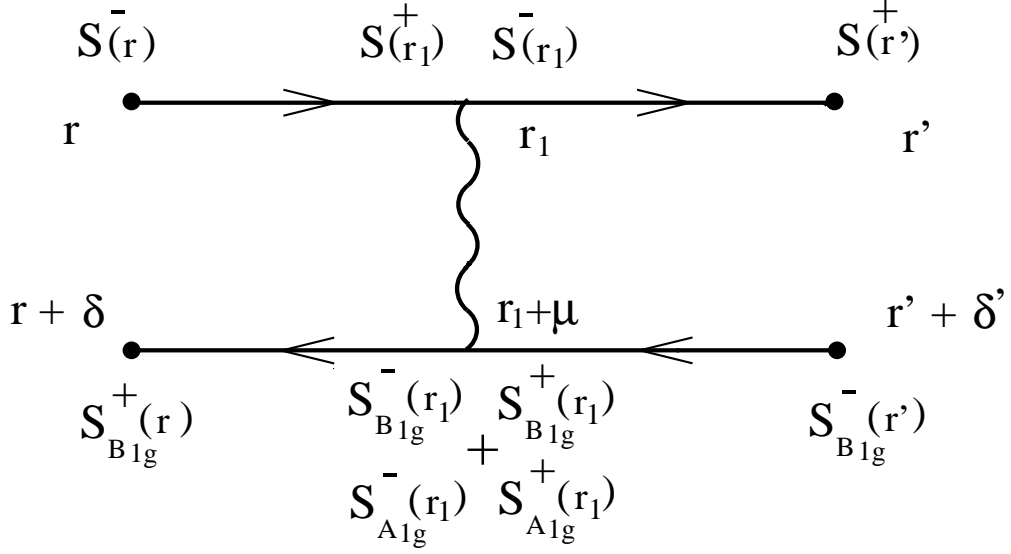


FIG. 1. Interaction between two magnons is shown where the bold lines represent the two magnons propagating from neighbouring sites \mathbf{r} and $\mathbf{r} + \delta$ to \mathbf{r}' and $\mathbf{r}' + \delta'$. The wavy lines denotes the interaction between the magnons at sites \mathbf{r}_1 and $\mathbf{r}_1 + \mu$ where μ connects to the nearest neighbouring sites. The creation and destruction of magnons at these points are shown by S^+ and S^- where the subscripts B_{1g} and A_{1g} correspond to different scattering geometries defined in the text.

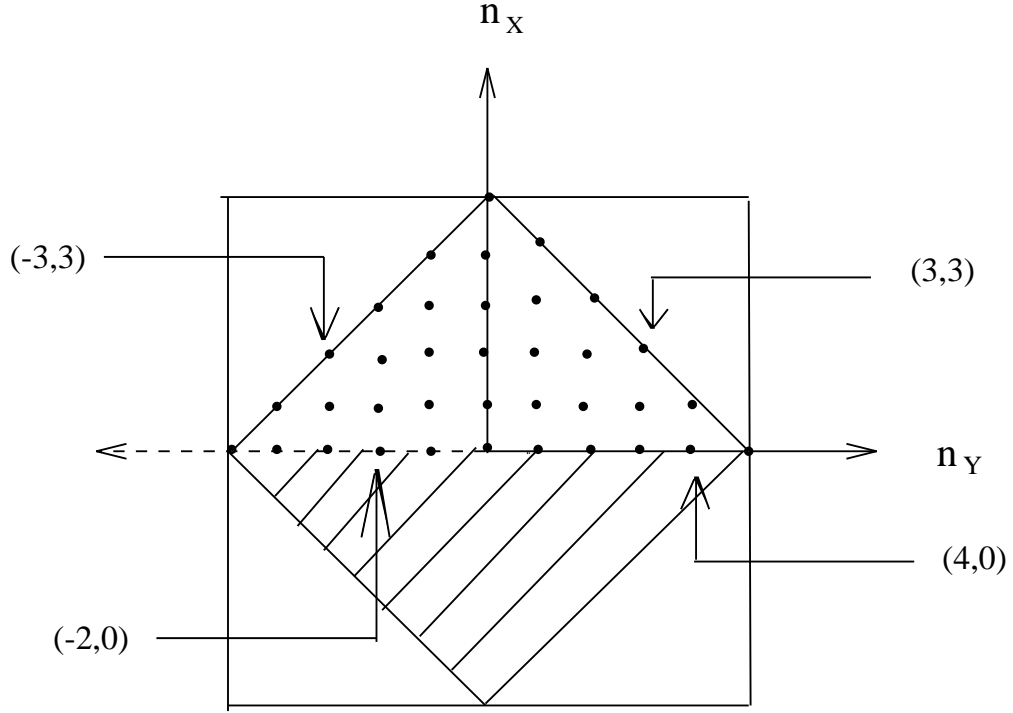


FIG. 2. The region in the Brillouin Zone (BZ) is shown where the dots denote the mode numbers n_x and n_y chosen so as to assign labels to the mode energies calculated. A few of the mode numbers are indicated. The first two quadrants are required for assigning numbers to all the modes.

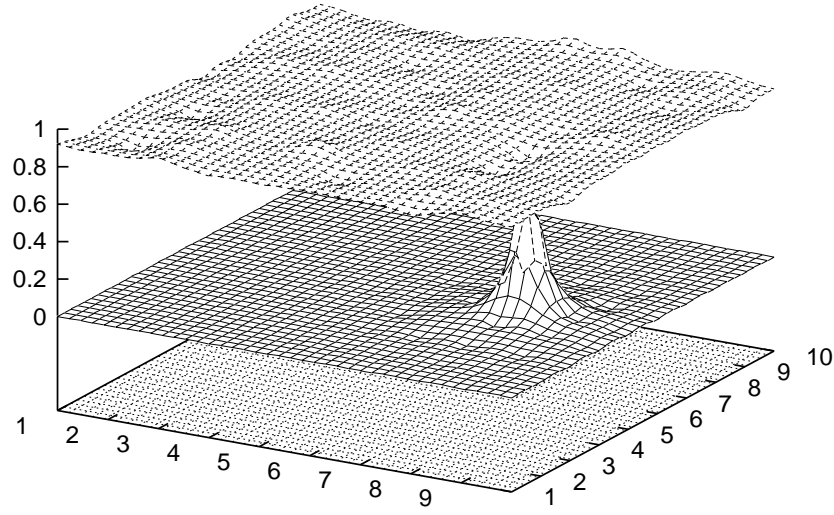


FIG. 3. The amplitude for the highest energy magnon mode (below) is shown for a 10×10 lattice for $U/t = 10$ in presence of disorder $\sigma = 0.1$. Also we have shown the magnetization profile (top) which shows a dip at places where the locally averaged hopping strength is maximum.

≡ ε

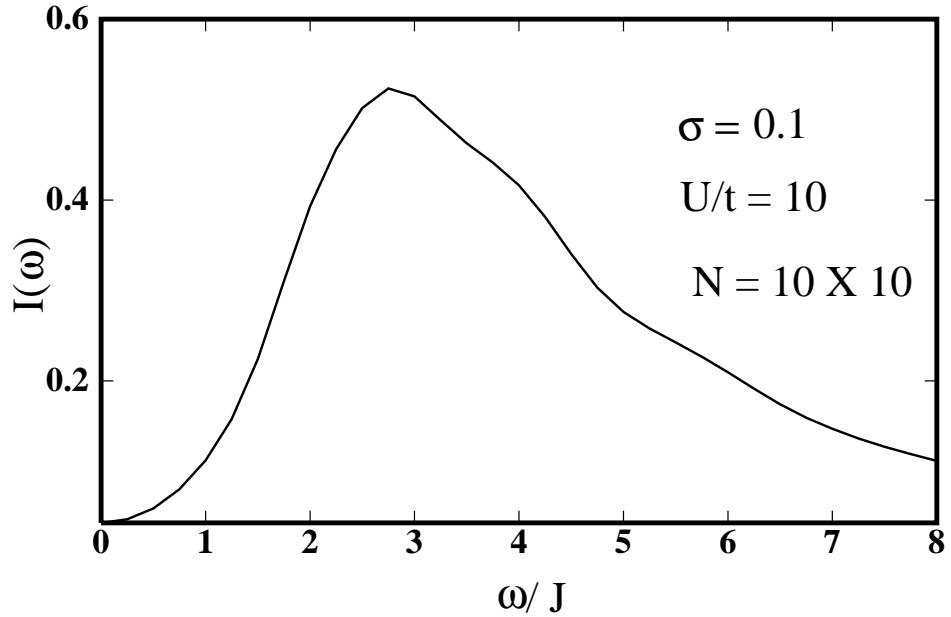


FIG. 4. The two-magnon scattering intensity is plotted as a function of transferred photon frequency ω (in units of J) for the hopping disordered case with a gaussian disorder of width $\sigma = 0.1$.

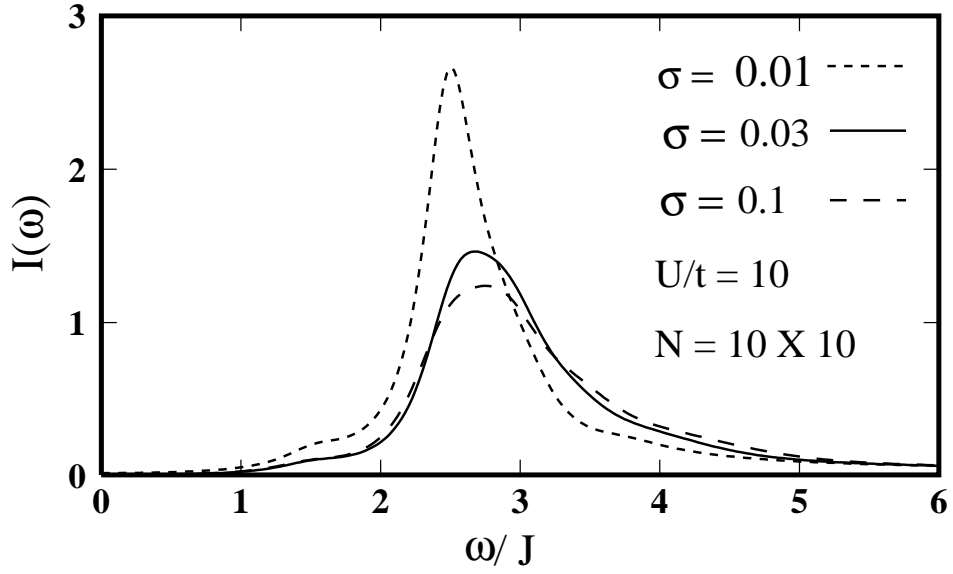


FIG. 5. The two-magnon Raman lineshape is shown for more moderate values of disorder, viz. $\sigma = 0.01$ and 0.03 . The pure case ($\sigma = 0.0$) is included for comparison

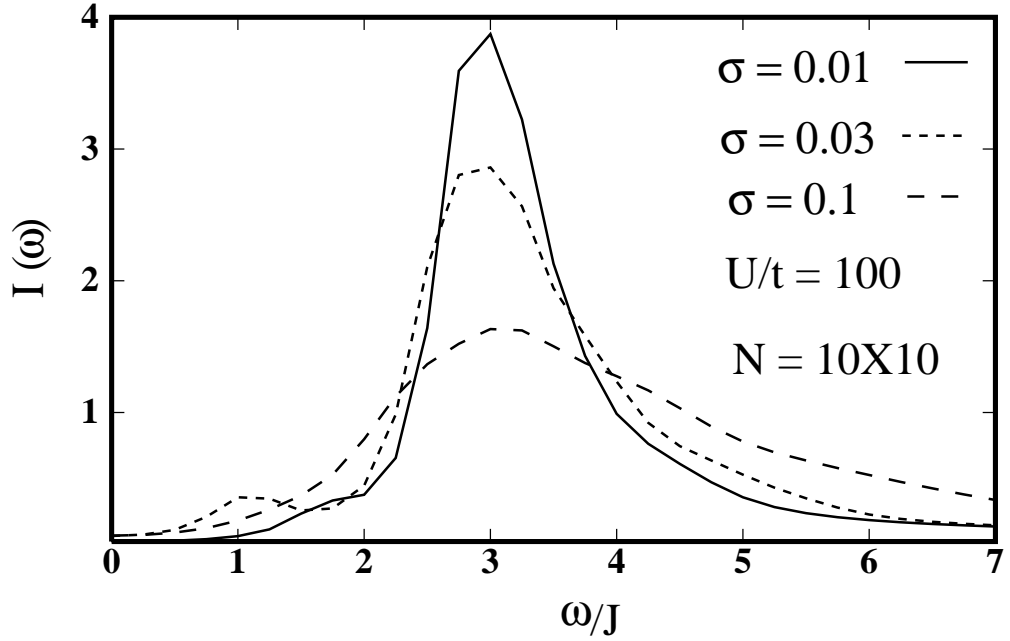


FIG. 6. The two-magnon Raman lineshape is shown for the strong coupling case ($U/t = 100$) in order to compare with the results of Reference [1]. The values taken for disorder are $\sigma = 0.01$, 0.03 and 0.1 .

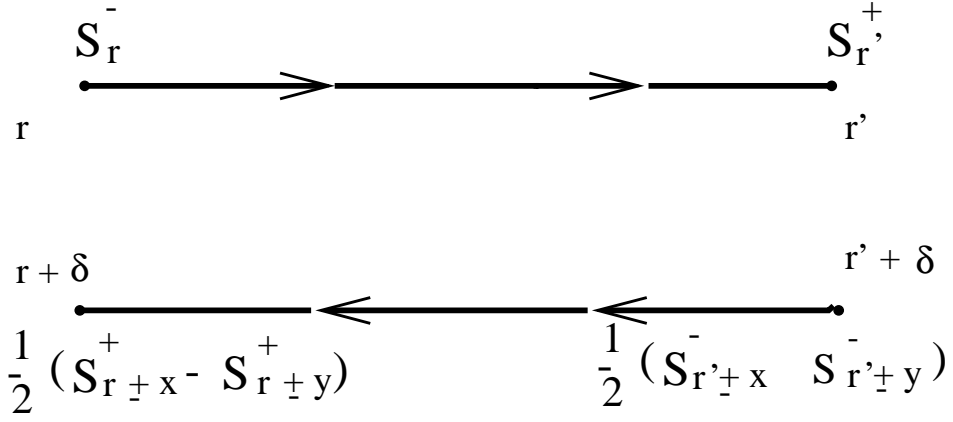


FIG. 7. The two-magnon Raman propagator in the non-interacting limit corresponding to the B_{1g} symmetry is shown.

TABLE I. The mode energies are obtained using the expression relevant to the intermediate- U regime ($U/t = 10$ or $\Delta/t = 5$) for a 10×10 system where $n_{x/y} = (\frac{L}{2\pi})q_{x/y}$ are the mode numbers specified in the leftmost column. Also we have shown the energies calculated numerically using the exact eigenstate method for comparison. The symmetry factors for both B_{1g} and A_{1g} scattering geometries are obtained using the mode numbers.

Mode Nos. (n_x, n_y)	ω_n (numerical)	ω_n (formula)	$\phi_n^2(B_{1g})$	$\phi_n^2(A_{1g})$
(-5,0)	0.7548	0.7505	4.000	0.000
(4,0) (0,4) (-4,0) (-5,1)	0.7438	0.7408	2.618	0.000
(4,1) (1,4) (-4,1) (-1,4)	0.7396	0.7356	0.382	0.000
(3,2) (2,3) (-3,2) (-2,3)	0.7150	0.6931	3.272	0.037
(3,1) (1,3) (-3,1) (-1,3)	0.7030	0.6927	1.250	0.250
(4,2) (2,4) (-4,2) (-2,4)				
(3,0) (0,3) (-3,0) (-5,2)	0.6882	0.6793	0.000	0.382
(2,2) (3,3) (-2,2) (-3,3)	0.6765	0.6696	1.713	0.478
(2,1) (1,2) (-2,1) (-1,2)	0.5945	0.5826	0.250	1.250
(4,3) (3,4) (-4,3) (-3,4)				
(2,0) (0,2) (-2,0) (-5,3)	0.5469	0.5458	0.477	1.714
(1,1) (4,4) (-1,1) (-4,4)	0.4199	0.4102	0.000	2.618
(1,0) (0,1) (-1,0) (-5,4)	0.3061	0.2987	0.036	3.273
(0,0)	0.0000	0.0000	0.000	4.000

TABLE II. Here the assignment of the mode numbers n_x and n_y is shown for the mode energies calculated numerically for both pure and disordered systems ($\sigma = 0.1$) of size 10×10 and for $U/t = 10$.

Mode Nos. (n_x, n_y)	ω_n (pure case)	ω_n (disordered case)
(-5,0)	0.7548	1.3006
(4,0) (0,4) (-4,0) (-5,1)	0.7438	1.2222, 1.2024, 1.1960, 1.1346
(4,1) (1,4) (-4,1) (-1,4)	0.7396	1.0578, 1.0178, 1.0137, 0.9955
(3,2) (2,3) (-3,2) (-2,3)	0.7150	0.8557, 0.8414, 0.8291, 0.7934
(3,1) (1,3) (-3,1) (-1,3)	0.7030	0.7854, 0.7762, 0.7698, 0.7641
(4,2) (2,4) (-4,2) (-2,4)		0.7228, 0.7018, 0.6935, 0.6624
(3,0) (0,3) (-3,0) (-5,2)	0.6882	0.6614, 0.6554, 0.6364, 0.6197
(2,2) (3,3) (-2,2) (-3,3)	0.6765	0.6020, 0.5773, 0.5668, 0.5411
(2,1) (1,2) (-2,1) (-1,2)	0.5945	0.5251, 0.5167, 0.4926, 0.4784
		0.4527, 0.4361, 0.4256, 0.4151
(2,0) (0,2) (-2,0) (-5,3)	0.5469	0.3969, 0.3711, 0.3595, 0.3424
(1,1) (4,4) (-1,1) (-4,4)	0.4199	0.3320, 0.3170, 0.2909, 0.2778
(1,0) (0,1) (-1,0) (-5,4)	0.3061	0.2390, 0.2118, 0.1801, 0.1643
(0,0)	0.0000	0.0000

ACKNOWLEDGMENT

I am thankful to Dr. Avinash Singh for his insightful comments regarding the manuscript. The work has been supported by a Research Grant SP/S2/M-25/95 from the Department of Science and Technology (DST), India.

-
- [1] F.Nori, R. Merlin, S. Haas, A.W. Sandvik and E. Dagotto, Phys. Rev. Lett. **75**, 553 (1995)
 - [2] F. Scönfeld, A.P. Kampf and E. Müller Hartmann, Z. Phys. B **102**, 25 (1997)
 - [3] S.Basu and A.Singh, Phys. Rev. B **55**, 12338 (1997)
 - [4] S. Basu and A. Singh, Phys. Rev. B **53**, 6406 (1996)
 - [5] A. Singh, M. Ulmke and D. Vollhardt, Report Number 9803094
 - [6] B.S. Shastry and B.I. Shraiman, Int. J. Mod. Phys. B, **5**, 365 (1991)
They have also pointed out that only diagonal terms contribute to the scattering rate because of the lattice symmetry.
 - [7] S. Basu and A. Singh, Phys. Rev. B **54**, 6356 (1996)
 - [8] R.R.P. Singh, P.A. Fleury, K.B. Lyons and P.E. Sulewski, Phys. Rev. Lett. **62**, 2736 (1989)